Intelligent Sensor Fault Detection and Isolation in Industrial System: A Data-Model Interactive Subspace Approach

Shenquan Wang and Di Meng

***Abstract*—This paper proposes a novel intelligent fault detection method, i.e., combining the subspace identification technique (SIT) with the data-model interactive compensation mechanism for fault detection. More precisely, the design process is divided into two primary stages: offline learning process and real-time fault monitoring. In the offline learning phase, the fault isolation algorithm is employed, along with parameter identification using the subspace identification technique. Then the online data undergo normalization processing and are subjected to online fault detection using a trained offline model. In addition, considering the accuracy of fault detection, this paper designs the dynamic optimal threshold based on the fault detection rate (FDR) and the false alarm rate (FAR). In the end, the case studies on PT700 and Tennessee Eastman (TE) process data are provided to confirm that the proposed method achieves the fault detection objectives.**

***Index Terms*—Subspace identification technique, intelligent fault detection, data-model interaction, optimal threshold**

I. INTRODUCTION

As modern science and technology advance swiftly, particularly in aerospace, aviation, nuclear industry, and high-speed railway sectors, the scale and complexity of industrial systems have significantly increased. As a result, component faults have become inevitable due to complex system structures, continuous heavy workloads, and changing external conditions. Undetected faults can degrade system performance and may even lead to catastrophic consequences, underscoring the necessity of fault detection (FD) technology. In most industrial systems, sensors are crucial for perceiving the external environment and determining the core capabilities of intelligent devices. Reliable sensor measurements are essential for system status monitoring, but sensor accuracy can decline over time due to environmental influences, leading to various types of faults. If sensor errors are not detected promptly, they can result in significant industrial accidents. Prompt detection of sensor faults is, therefore, crucial for maintaining the safety and stability of system operations.

Sensor fault detection methods in industrial systems are mainly divided into model-based methods and data-based methods. A model-based fault detection scheme is an effective tool for different types of sensor fault detections, such as bias, gain, drift, card faults, etc. [1–7]. This method relies on accurate mathematical models to describe the dynamic behavior of the system. However, due to the complex structure and uncertainty of industrial systems, it is often challenging to develop precise models. The main drawback of this approach is that inaccuracies in the model can lead to decreased fault detection performance, making it difficult to handle complex operating conditions and system dynamics. Consequently, data-driven detective methods have gained increasing attention. These methods utilize a large number of historical data and advanced algorithms for fault detection, effectively addressing the complexity and uncertainty of industrial systems and providing more flexible and accurate detective results.

Data-driven fault detection methods mainly include machine learning methods, signal processing methods, and multivariate statistical analysis methods. Machine learning based fault detection methods can handle complex data and build highly robust predictive models, offering advantages in automation and intelligence [8–10]. However, these methods have high computational complexity and are heavily dependent on the quality and quantity of data. Signal processing based fault detection methods have strong feature extraction capabilities, allowing real-time data analysis and aiding in online monitoring and fault detection [11]. However, these methods heavily rely on expert knowledge. Multivariate statistical analysis based fault detection methods can handle high-dimensional datasets and effectively extract key fault features from sensor data [12–14]. However, they have high requirements for data quality, and noise, missing values, and outliers can significantly impact diagnostic performance.

In summary, to fully leverage the advantages of various fault detection methods, Ref. [15] proposes a data-model interactive fault detection method based on subspace identification technique (SIT). Subspace identification technique does not require priori system models. It only requires extracting useful information from a substantial volume of input-output (I/O) data, avoiding the challenges of model parameterization and nonlinear optimization. This effectively addresses the problems of difficulty in model building and poor data quality. Although subspace identification techniques are robust to a certain extent of noise, their recognition accuracy may decrease when noise levels are high, affecting diagnostic reliability. Moreover, setting threshold usually relies on empirical adjustments,

Manuscript received: 24 May 2024; revised: 17 July 2024; accepted: 29 August 2024. *(Corresponding author: Shenquan Wang.)*

Citation: S. Wang and D. Meng, Intelligent sensor fault detection and isolation in industrial system: A data-model interactive subspace approach, *IJICS*, 2024, 29(3), 119–126.

Shenquan Wang and Di Meng are with College of Electrical and Electronic Engineering, Changchun University of Technology, Changchun 130012, China (e-mail: shenquanwang@126.com; dimeng127@163.com).

Digital Object Identifier 10.62678/IJICS202409.10128

lacking systematic guidelines. Therefore, it is necessary to develop a new intelligent fault detection technology to address the aforementioned issues.

Driven by the previous discussions, this article aims to design a new intelligent fault detection technology based on complex sensor signals under data-model interactive compensation. First, the sensor data collected under normal operating conditions are standardized to eliminate the influence of varying dimensions. Next, the data are partitioned and reduced in dimensionality using a moving window (MW) method, allowing for the extraction of main feature vectors to form a low-dimensional subspace model for fault detection. Based on this model, singular value decomposition (SVD) is applied to obtain the equivalent vectors of the input and output data, which are then used to construct residuals. Subsequently, an isolation algorithm is employed to generate specific residuals for each sensor. Finally, a dynamic threshold is designed to achieve comprehensive fault detection. The main contributions of this paper are as follows:

(1) Based on subspace identification technique, an intelligent sensor fault detection scheme is designed under data-model interactive compensation, and the implementation of the proposed scheme only requires system I/O data.

(2) The phase of offline learning builds specific residuals for each sensor and locates the faulty sensor.

(3) A threshold optimization method based on subspace identification technique is proposed. By analyzing the residual distribution of normal data, the optimal threshold is found to minimize the false alarm rate (FAR).

The remainder of the paper is structured as follows. Section II states subspace identification technique for fault detection fundamentals. In Section III, intelligent fault detection schemes are discussed. The experimental verification is provided in Section IV. Finally, this paper is concluded in Section V.

II. Subspace Identification Technique for Fault Detection Fundamental

Take into account the following discrete linear time-invariant system

$$\begin{aligned} x(k+1) &= Ax(k) + Bu(k) + w(k), \\ y(k) &= Cx(k) + Du(k) + v(k) \end{aligned} \tag{1}$$

where k represents the sequence of time in a discrete-time system, and A, B, C, and D are matrices. $x(k) \in \mathbb{R}^n$, $u(k) \in \mathbb{R}^l$, and $y(k) \in \mathbb{R}^m$ are the state vector, input vector, and output vector, with dimensions n, l, and m, respectively. $w(k) \in \mathbb{R}^n$ and $v(k) \in \mathbb{R}^m$ are assumed to be process noise and sensor noise satisfying

$$\begin{aligned} &E\left(\begin{bmatrix} w(i) \\ v(i) \end{bmatrix}\begin{bmatrix} w^{\mathrm{T}}(j) & v^{\mathrm{T}}(j) \end{bmatrix}\right) = \begin{bmatrix} Q & S \\ S^{\mathrm{T}} & R \end{bmatrix}\delta_{ij}, \\ &\delta_{ij} = \begin{cases} 1, & i = j; \\ 0, & i \neq j \end{cases} \end{aligned} \tag{2}$$

where $E(\cdot)$ is the expectation operator, and $i, j \in N$, N represents the number of consecutive data points extracted for analysis.

It is assumed that the system matrices A, B, C, and D, the system order n, and the matrices Q, R, and S are unknown a priori. Additionally, these elements are statistically independent of the input vector $u(k)$ and the initial state $x(0)$. The following data structures will be utilized.

$$X(j) = [x(j), x(j+1), \ldots, x(j+N-1)] \in \mathbb{R}^{n\times N} \tag{3}$$

$$U(j) = [u(j), u(j+1), \ldots, u(j+N-1)] \in \mathbb{R}^{l\times N} \tag{4}$$

$$Y(j) = [y(j), y(j+1), \ldots, y(j+N-1)] \in \mathbb{R}^{m\times N} \tag{5}$$

$$W(j) = [w(j), w(j+1), \ldots, w(j+N-1)] \in \mathbb{R}^{n\times N} \tag{6}$$

$$V(j) = [v(j), v(j+1), \ldots, v(j+N-1)] \in \mathbb{R}^{m\times N} \tag{7}$$

$$U_p = \left[U^{\mathrm{T}}(i-s_p), U^{\mathrm{T}}(i-s_p+1), \ldots, U^{\mathrm{T}}(i-1)\right]^{\mathrm{T}} \in \mathbb{R}^{s_p l\times N} \tag{8}$$

$$Y_p = \left[Y^{\mathrm{T}}(i-s_p), Y^{\mathrm{T}}(i-s_p+1), \ldots, Y^{\mathrm{T}}(i-1)\right]^{\mathrm{T}} \in \mathbb{R}^{s_p m\times N} \tag{9}$$

$$U_f = \left[\ U^{\mathrm{T}}(i), U^{\mathrm{T}}(i+1), \ldots, U^{\mathrm{T}}(i+s_f-1)\ \right]^{\mathrm{T}} \in \mathbb{R}^{s_f l\times N} \tag{10}$$

$$Y_f = \left[\ Y^{\mathrm{T}}(i), Y^{\mathrm{T}}(i+1), \ldots, Y^{\mathrm{T}}(i+s_f-1)\ \right]^{\mathrm{T}} \in \mathbb{R}^{s_f m\times N} \tag{11}$$

$$\begin{aligned} Z_p &= \begin{bmatrix} Y_p \\ U_p \end{bmatrix} \in \mathbb{R}^{(s_p l+s_p m)\times N}, \\ Z_f &= \begin{bmatrix} Y_f \\ U_f \end{bmatrix} \in \mathbb{R}^{(s_f l+s_f m)\times N} \end{aligned} \tag{12}$$

$$W_f = \left[\ W^{\mathrm{T}}(i), W^{\mathrm{T}}(i+1), \ldots, W^{\mathrm{T}}(i+s_f-1)\ \right]^{\mathrm{T}} \in \mathbb{R}^{s_f n\times N} \tag{13}$$

$$V_f = \left[\ V^{\mathrm{T}}(i), V^{\mathrm{T}}(i+1), \ldots, V^{\mathrm{T}}(i+s_f-1)\ \right]^{\mathrm{T}} \in \mathbb{R}^{s_f m\times N} \tag{14}$$

where subscripts p and f signify past and future data, respectively.

Equation (1) can be brought into

$$Y_f = \mathfrak{A}_{\mathrm{s}} X(i) + H_{\mathrm{s,u}} U_f + H_{\mathrm{s,w}} W_f + V_f \tag{15}$$

where $X(i)$ indicates state data matrix at time step i, and subscripts s, u, and w indicate state, input, and process noise, and

$$H_{\mathrm{s,u}} = \begin{bmatrix} D & 0 & \ldots & 0 & 0 \\ CB & D & \ldots & 0 & 0 \\ \vdots & \vdots & \ddots & \vdots & \vdots \\ CA^{s_f-3}B & CA^{s_f-4}B & \ldots & D & 0 \\ CA^{s_f-2}B & CA^{s_f-3}B & \ldots & CB & D \end{bmatrix},$$

$$H_{\mathrm{s,w}} = \begin{bmatrix} 0 & 0 & \ldots & 0 & 0 \\ C & 0 & \ldots & 0 & 0 \\ \vdots & \vdots & \ddots & \vdots & \vdots \\ CA^{s_f-3} & CA^{s_f-4} & \ldots & 0 & 0 \\ CA^{s_f-2} & CA^{s_f-3} & \ldots & C & 0 \end{bmatrix},$$

$$\mathfrak{A}_{\mathrm{s}} = \begin{bmatrix} C \\ CA \\ \vdots \\ CA^{s_f-1} \end{bmatrix},$$

the block Hankel matrices for subsequent outputs and inputs are denoted by Y_f and U_f, respectively. The observability matrix is represented by $\mathfrak{A}_\mathrm{s}$. Moreover, W_f and V_f denote the block Hankel matrices corresponding to process noise and sensor noise, respectively. s_p and s_f stand for integers with $s_p > n$ and $s_f > n$.

Z_f can be rewritten in another form according to Eq. (15)

$$\begin{aligned} Z_f &= \begin{bmatrix} \mathfrak{A}_\mathrm{s} & H_\mathrm{s,u} \\ 0 & I \end{bmatrix} \begin{bmatrix} X(i) \\ U_f \end{bmatrix} + \psi, \\ \psi &= \begin{bmatrix} H_\mathrm{s,w} W_f + V_f \\ 0 \end{bmatrix} \end{aligned} \tag{16}$$

where I is the unit matrix.

Pre-multiplying Z_f by $1/N$ and post-multiplying by Z_p^T, one has

$$\frac{1}{N} Z_f Z_p^\mathrm{T} = \frac{1}{N} \begin{bmatrix} \mathfrak{A}_\mathrm{s} & H_\mathrm{s,u} \\ 0 & I \end{bmatrix} \begin{bmatrix} X(i) \\ U_f \end{bmatrix} Z_p^\mathrm{T} + \frac{1}{N} \psi Z_p^\mathrm{T}.$$

For $N \to +\infty$, we have $\psi Z_p^\mathrm{T}/N = 0$. The covariance matrix undergoes SVD

$$\frac{1}{N} Z_f Z_p^\mathrm{T} = U_\mathrm{z} \Sigma V_\mathrm{z},$$

with unitary matrix

$$U_\mathrm{z} = \begin{bmatrix} U_{\mathrm{z},11} & U_{\mathrm{z},12} \\ U_{\mathrm{z},21} & U_{\mathrm{z},22} \end{bmatrix} \tag{17}$$

where z indicates z-domain, V_z is an orthogonal matrix, $U_{\mathrm{z},11} \in \mathbb{R}^{ms_f \times (ls_f + n)}$, $U_{\mathrm{z},12} \in \mathbb{R}^{ms_f \times (ms_f - n)}$, and $U_{\mathrm{z},22} \in \mathbb{R}^{ls_f \times (ms_f - n)}$, respectively.

$\mathfrak{A}_\mathrm{s}^\perp$ and $\mathfrak{A}_\mathrm{s}^\perp H_\mathrm{s,u}$ are obtained using the following relations

$$\begin{aligned} \mathfrak{A}_\mathrm{s}^\perp &= U_{\mathrm{z},12}^\mathrm{T}, \\ \mathfrak{A}_\mathrm{s}^\perp H_\mathrm{s,u} &= -U_{\mathrm{z},22}^\mathrm{T} \end{aligned} \tag{18}$$

As demonstrated in Ref. [16], the entire identification process must adhere to

$$\mathrm{rank}\left(\frac{1}{N} \begin{bmatrix} X(i) \\ U_f \end{bmatrix} Z_p^\mathrm{T} \right) = n + s_f l \tag{19}$$

The parity vector $\alpha_\mathrm{s} \in \mathbb{R}^{(s+1)m}$, where the superscript s indicates the order of the parity space, is first determined using the following procedure

$$\alpha_\mathrm{s} \mathfrak{A}_\mathrm{s} = 0 \tag{20}$$

where $\alpha_\mathrm{s} = [\alpha_{\mathrm{s},0}, \alpha_{\mathrm{s},1}, \ldots, \alpha_{\mathrm{s},i}]$, $\alpha_{\mathrm{s},i} \in \mathbb{R}^m$ and $i = 0, 1, ..., s$.

From Eq. (15), it can be derived that

$$Z_f^\perp Z_f Z_p^\mathrm{T} = 0 \Rightarrow Z_f^\perp \begin{bmatrix} \mathfrak{A}_\mathrm{s} & H_\mathrm{s,u} \\ 0 & I \end{bmatrix} = 0 \tag{21}$$

Thus, the rank of matrix $\mathfrak{A}_\mathrm{s}^\perp$ can be determined as

$$\mathrm{rank}(Z_f^\perp) = sm - n > 0 \tag{22}$$

Subsequently, the residual generator can be formulated as

$$r(k) = \alpha_\mathrm{s}(y_\mathrm{s}(k) - H_\mathrm{s,u} u_\mathrm{s}(k)) \tag{23}$$

where y_s represents the observed value of the output of the system and u_s represents external input applied to the system.

III. Intelligent Fault Detection Scheme

A. SIT Based on MW

A key challenge in sensor fault detection is that the sample variables do not change significantly. To overcome this challenge, the MW technique is employed to aggregate samples over a defined period, enhancing deviations caused by sensor faults. Initially, the sample is normalized, and the value of the measured data point from a sensor q_k at time k is expressed as s_k

$$s_k = q_k + q_{k-1} + \cdots + q_{k-\mathrm{dc}+1},$$

where dc refers to the window size. After applying MW, the sample q_k is transformed into the processed value s_k, which simplifies to q_k when $\mathrm{dc} = 1$. The steps of the MW-SIT method are outlined as follows:

Step 1 Dataset Q is standardized.

Step 2 The sample set S is generated from Q using the MW method, with a window size of dc.

Step 3 Using SIT, the model is trained, and its critical value, J_th, is ascertained through the Chi-square statistical method.

Step 4 Real-time data are standardized.

Step 5 Utilizing the same MW technique applied to historical samples, a new sample s_new can be derived from the real-time data q_new.

Step 6 The newly acquired sample s_new is inserted into the offline MW-SIT framework to produce the residual signal.

B. Fault Isolation

Fault isolation refers to the process of identifying which specific sensor has malfunctioned. The underlying algorithm operates by establishing a parity space for each sensor in a way, so that its impact on the corresponding residual is entirely independent of the influence of other sensors. The fault isolation algorithm is detailed as follows [17]:

Step 1 $\mathfrak{A}_\mathrm{s}^\perp$ and $\mathfrak{A}_\mathrm{s}^\perp H_\mathrm{s,u}$ are extracted from I/O data of the process.

Step 2 $\mathfrak{A}_\mathrm{s}^\perp$ is distributed as

$$\mathfrak{A}_\mathrm{s}^\perp = \left[\mathfrak{A}_{\mathrm{s},1}^\perp, \mathfrak{A}_{\mathrm{s},2}^\perp, \ldots, \mathfrak{A}_{\mathrm{s},t}^\perp \right],$$

where $\mathfrak{A}_{\mathrm{s},t}^\perp \in \mathbb{R}^{\mu \times m}$, $t = 1, 2, \ldots, s_\mathrm{a}$ and $\mu = ms_f - n$.

Step 3 Now $\mathfrak{A}_{\mathrm{s},t}^\perp$ is subdivided as

$$\mathfrak{A}_{\mathrm{s},t}^\perp = \left[\mathfrak{A}_{\mathrm{s},t,1}^\perp, \mathfrak{A}_{\mathrm{s},t,2}^\perp, \ldots, \mathfrak{A}_{\mathrm{s},t,i}^\perp \right],$$

where $\mathfrak{A}_{\mathrm{s},t,i}^\perp \in \mathbb{R}^{\mu \times 1}$ and $i = 1, 2, \ldots, m$.

Step 4 Next, $\mathfrak{A}_{\mathrm{s},t,i}^\perp$ is rearranged to eliminate the influence of other sensors.

$$\begin{aligned} \mathfrak{A}_{\mathrm{s},t,\tilde{i}}^\perp = \big[& \mathfrak{A}_{\mathrm{s},1,1}^\perp, \mathfrak{A}_{\mathrm{s},1,2}^\perp, \ldots, \mathfrak{A}_{\mathrm{s},1,i-1}^\perp, \mathfrak{A}_{\mathrm{s},1,i+1}^\perp, \ldots, \mathfrak{A}_{\mathrm{s},1,m}^\perp, \ldots, \\ & \mathfrak{A}_{\mathrm{s},s_\mathrm{a},1}^\perp, \mathfrak{A}_{\mathrm{s},s_\mathrm{a},2}^\perp, \ldots, \mathfrak{A}_{\mathrm{s},s_\mathrm{a},i-1}^\perp, \mathfrak{A}_{\mathrm{s},s_\mathrm{a},i+1}^\perp, \ldots, \mathfrak{A}_{\mathrm{s},s_\mathrm{a},m}^\perp \big], \end{aligned}$$

where $\tilde{i}$ represents the rearranged position of sensor i after decoupling the effect of other sensors.

Step 5 $S_{\mathrm{sen},i} \mathfrak{A}_{\mathrm{s},t,\tilde{i}}^\perp = 0$ is solved to obtain $S_{\mathrm{sen},i}$, where $S_{\mathrm{sen},i}$ is the projection matrix.

Step 6 The parity space for the i-th sensor $\mathfrak{A}_{\mathrm{s,sen},i}^\perp$ is determined by using the equation $\mathfrak{A}_{\mathrm{s,sen},i}^\perp = S_{\mathrm{sen},i} \mathfrak{A}_\mathrm{s}^\perp$.

Step 7 Build residuals for the i-th sensor using the following equation

$$r_{\text{sen},i}(t) = a_{\text{sen},i}(y_{\text{s}}(t) - H_{\text{s,u}}u_{\text{s}}(t)),$$

where $a_{\text{sen},i}$ is the parity vector of the i-th sensor and $a_{\text{sen},i} = S_{\text{sen},i}\mathfrak{N}_{\text{s}}^{\perp}$.

Step 8 Referring to the χ^2 test table, find χ_α such that $\text{prob}[\chi > \chi_\alpha] = \alpha$ to establish the permissible limit for FAR, where χ is a random variable that follows the Chi-squared distribution, χ_α is the critical value at a given confidence level, and α is a confidence level.

Step 9 The threshold is set as $J_{\text{th}} = \chi_\alpha/2$.

Step 10 The testing statistics are represented by $J = \dfrac{1}{2\sigma^2 N_{\text{w}}}\left(\sum_{i=1}^{N_{\text{w}}} r_{\text{sen},i}^2\right)$, where σ is the variance of residuals and N_{w} is the number of samples in MW.

Step 11 Determine as follows:

$$J \leqslant J_{\text{th}} \implies \text{no fault},$$
$$J > J_{\text{th}} \implies \text{fault detected}.$$

C. Dynamic Optimal Threshold

This section outlines the steps to optimize the threshold for fault detection using a subspace-based residual generator, which are detailed as follows:

Step 1 Sensor data are normalized to eliminate the impact of different units.

Step 2 The MW method is used to divide the standardized data for analysis.

Step 3 SVD is applied to extract key features from the I/O data.

Step 4 Residuals are created using the extracted features for fault detection.

Step 5 While ensuring the fault detection rate (FDR), FAR is determined under different thresholds to identify the optimal threshold.

$$\text{FAR}(J) = \frac{1}{n}\sum_{i=1}^{n} 1(r_i > J),$$

$$J_{\text{opt}} = \arg\min_{J} \text{FAR}(J),$$

where $1(\cdot)$ is the indicator function, r_i indicates the residual value of sample i, and n is the number of samples.

Step 6 The threshold is adjusted dynamically based on real-time data changes.

Step 7 Real-time detection is implemented using the optimized threshold

$$J \leqslant J_{\text{opt}} \Rightarrow \text{no fault},$$
$$J > J_{\text{opt}} \Rightarrow \text{fault detected}.$$

IV. Experimental Verification

In this section, the effectiveness of the developed method is evaluated through the Tennessee Eastman (TE) process platform (as shown in Fig. 1) and the PT700 bearing load life testing apparatus (as shown in Fig. 2).

A. TE Process

The TE experimentation is capable of replicating 21 types

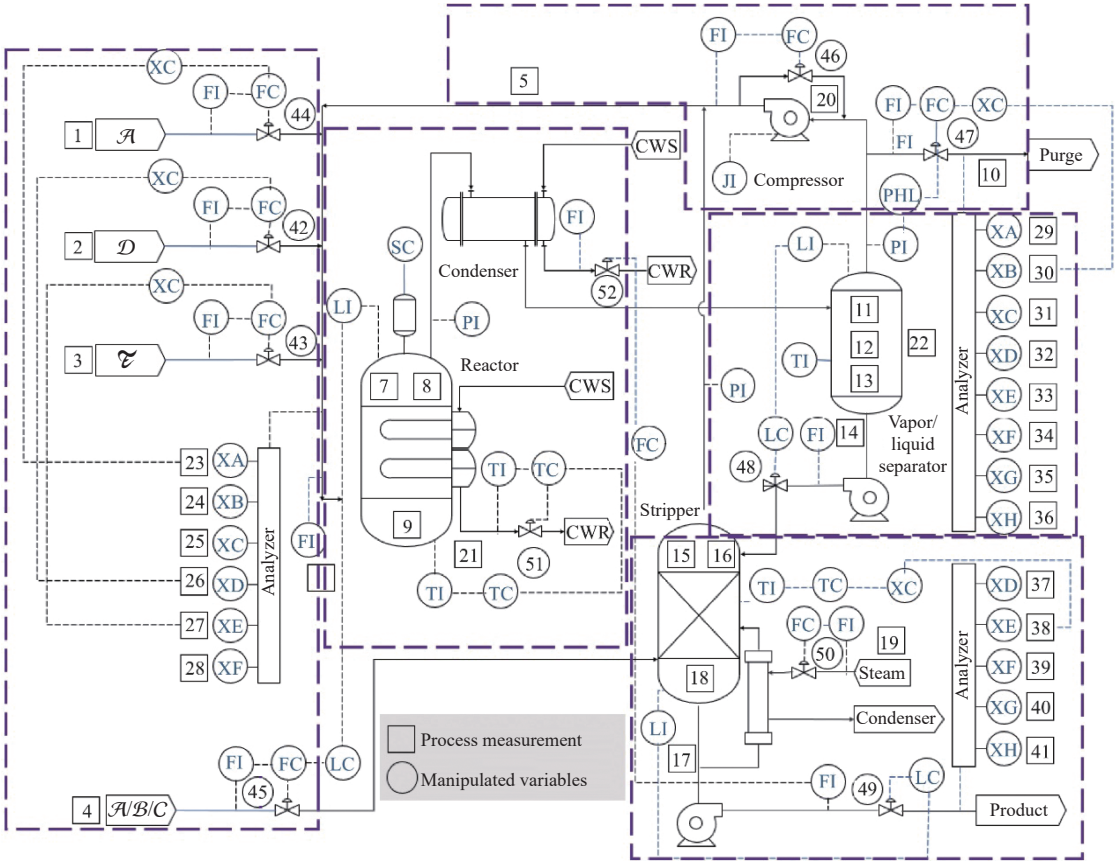

Figure 1 TE process.

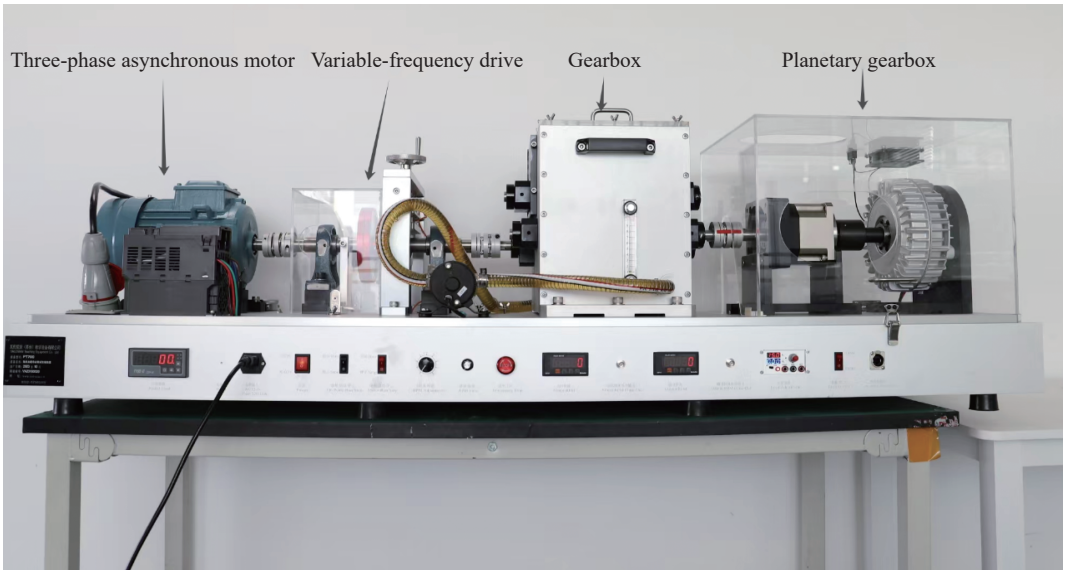

Figure 2 PT700 bearing load life testing apparatus.

of faults, as delineated in Table 1. For the faulted test set, the samples are derived from an experimentation run over 48 h with the fault induction occurring at the 8-h juncture. A compilation of 960 observations is amassed, of which the initial 160 observations represent the normal operational data.

To implement the proposed solution, the fault-free training datasets are initially used in the offline learning phase. Through offline learning, the observation matrix $\mathfrak{U}_s^{\perp}$ and the triangular matrix $H_{s,u}$ are identified. In this case study, we set a confidence level of 0.1 and choose data of fault 1 and fault 7 in Table 1 for experimentation verification. Specifically, assuming $p = f = 5$ and $N = 100$, the Hankel matrices U_p and $U_f \in \mathbb{R}^{55\times100}$ and Y_p and $Y_f \in \mathbb{R}^{20\times100}$ are derived through SVD.

Table 1 TE process fault description.

Fault No.	Fault description	Symbol
1	$\mathcal{A}/C$ feed flow ratio shifting, while component $\mathcal{B}$ content staying constant (flow 4)	Step
2	Component $\mathcal{B}$ content changing, but the $\mathcal{A}/C$ feed flow ratio staying the same (flow 4)	Step
3	Material $\mathcal{D}$ temperature variation (flow 2)	Step
4	Reactor cooling water inlet temperature fluctuation	Step
5	Condenser cooling water inlet temperature fluctuation	Step
6	Material $\mathcal{A}$ loss (flow 1)	Step
7	Material C pressure drop (flow 4)	Step
8	Changes in the composition of materials $\mathcal{A}$, $\mathcal{B}$, and C (flow 4)	Random variable
9	Material $\mathcal{D}$ temperature fluctuation (flow 2)	Random variable
10	Material C temperature fluctuation (flow 2)	Random variable
11	Reactor cooling water inlet temperature fluctuation	Random variable
12	Condenser cooling water inlet temperature fluctuation	Random variable
13	Changes in kinetic properties of the reaction	Slow drift
14	Reactor cooling water valve issue	Stiction
15	Condenser cooling water valve issue	Stiction
16	Unspecified issue	Unknown
17	Unspecified issue	Unknown
18	Unspecified issue	Unknown
19	Unspecified issue	Unknown
20	Valve for flow 4 remaining in a fixed position	Unknown
21	Valve for flow 4 remaining in a steady state position	Constant position

The results of fault detection are shown in Figs. 3–5, where J_1 represents the subspace identification technique with MW, J_2 is a subspace identification technique using MW technology and fault isolation algorithm, and J_3 is solely the subspace identification technique, respectively. As shown in Fig. 3, with an MW length of 3, the proposed method, which integrates subspace identification technique and fault isolation, performs exceptionally well and significantly outperforms the other two methods. This approach can detect faults promptly and accurately, effectively minimizing the impact of other sensors. Figure 4 demonstrates that for the same type of fault but with different MW lengths, the fault detection performance is considerably enhanced when the proposed method is applied. Figure 5 further indicates that for different types of faults under the same MW length, the fault detection capability improves even more with the addition of fault isolation. Moreover, the quantitative comparison of SIT, MW-SIT, and the proposed method, as presented in Table 2, evaluates the fault detection performance based on two criteria: FDR and FAR. The data in Table 2 clearly show that the proposed method significantly enhances fault detection performance. To further verify the effectiveness of the proposed solution, the method is applied to PT700 experimental platform for fault detection.

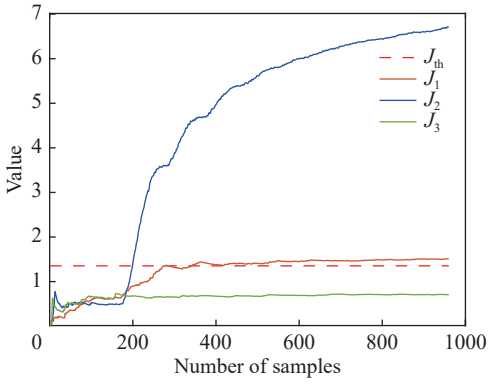

Figure 3 Fault detection result of fault 1: J_1 and J_2 with dc = 3, J_3 without.

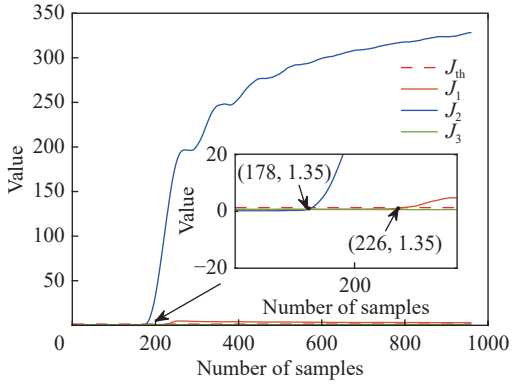

Figure 4 Fault detection result of fault 1: J_1 and J_2 with dc = 5, J_3 without.

B. PT700 Platform

In this experiment, real industrial data collected from the PT700 bearing load life testing apparatus are used. PT700 bearing fault types are shown in Table 3. Fault 3 in Table 3 is selected to validate the proposed solution. PT700 rolling element bearing failure refers to a crack of 0.5 or 0.3 mm on the rolling element. The fault frequency of the rolling element is 2.311 times the rotational frequency, but the defect in the rolling element occurs at twice the rotational speed because the rolling element is simultaneously impacted by both the inner and outer rings during one rotation.

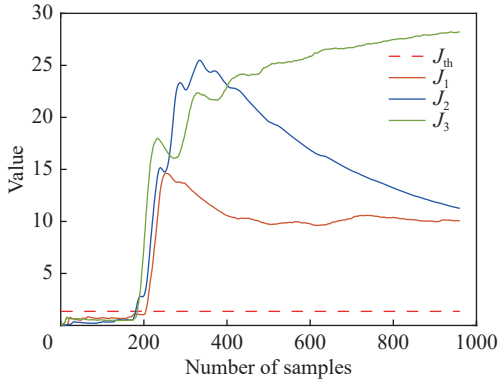

Figure 5 Fault detection result of fault 7: J_1 and J_2 with dc = 5, J_3 without.

Table 2 TE process fault detection result. Bold indicates the best detection result.

Fault No.	dc	Method	FDR	FAR
1	3	SIT	0.00	0.00
		MW-SIT	0.79	0.00
		Proposed method	**0.95**	**0.00**
	5	SIT	0.00	0.00
		MW-SIT	0.92	0.00
		Proposed method	**0.98**	**0.00**
7	5	SIT	0.97	0.00
		MW-SIT	0.94	0.00
		Proposed method	**0.98**	**0.00**

Table 3 PT700 bearing fault description.

Fault No.	Fault description	Fault characteristic frequency
1	Bearing inner ring fault	$5.430\mathcal{X}$
2	Bearing outer ring fault	$3.570\mathcal{X}$
3	Bearing rolling element fault	$4.622\mathcal{X}$
4	Bearing complex fault	Frequency of defects in outer and inner rings
5	Bearing cage fault	$0.397\mathcal{X}$

Note: $\mathcal{X}$ represents the multiple of shaft rotational frequency.

Initially, to implement the proposed scheme, a fault-free training dataset is used in the offline learning phase. Once this phase is completed, we can identify the observation matrix and the triangular matrix. Additionally, to ensure effective fault detection, rolling element bearing failure is injected at sample 200. Specifically, assuming $p = f = 5$ and $N = 100$, the Hankel matrices U_p and $U_f \in \mathbb{R}^{55\times100}$ and Y_p and $Y_f \in \mathbb{R}^{20\times100}$ are derived via SVD. The experimental results are shown in Figs. 6–8. The experimental results indicate that the

proposed method effectively accomplishes the fault detection task. Moreover, the proposed method demonstrates greater sensitivity to sensor faults, effectively reduces the FAR, and greatly improves the fault detection performance. The results of the tests are presented in Table 4. Through the comprehensive consideration of FDR and FAR, the proposed method is effective in the execution of fault detection tasks. In addition, to further enhance the effectiveness of fault detection, a dynamic optimal threshold is designed with FAR as the objective function, and the results are shown in Fig. 9. The detection results using the proposed method at the optimal threshold are shown in Fig. 10 and Table 5, with a window length of 200. Based on the experimental results, a significant improvement in fault detection performance can be observed.

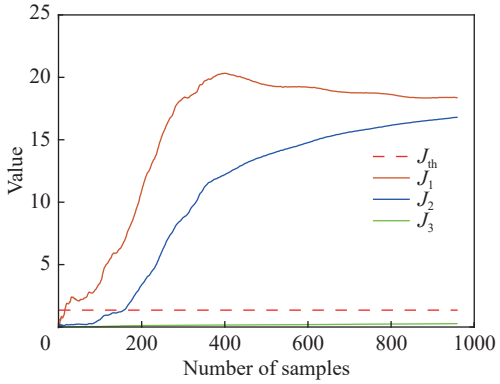

Figure 6 Fault detection result of PT700: J_1 and J_2 with dc = 200, J_3 without.

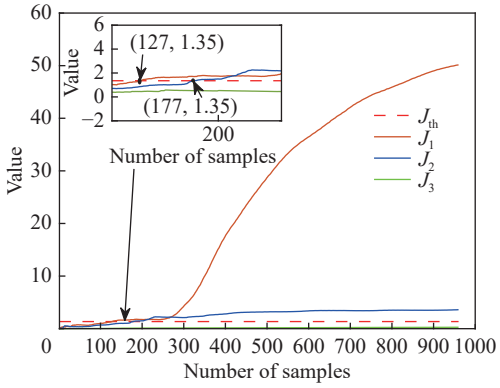

Figure 7 Fault detection result of PT700: J_1 and J_2 with dc = 160, J_3 without.

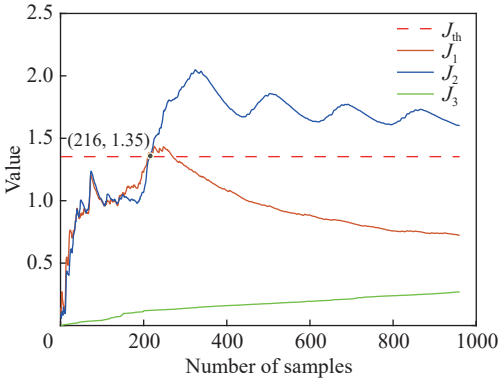

Figure 8 Fault detection result of PT700: J_1 and J_2 with dc = 70, J_3 without.

Table 4 PT700 fault detection result. Bold indicates the best detection result.

dc	Method	FDR	FAR
70	SIT	0.00	0.00
	MW-SIT	0.08	0.00
	Proposed method	**0.98**	**0.00**
160	SIT	0.00	0.00
	MW-SIT	1.00	0.37
	Proposed method	**1.00**	**0.11**
200	SIT	0.00	0.00
	MW-SIT	1.00	0.93
	Proposed method	**1.00**	**0.22**

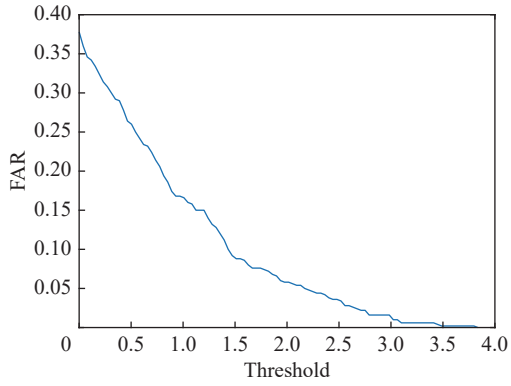

Figure 9 FAR vs. threshold.

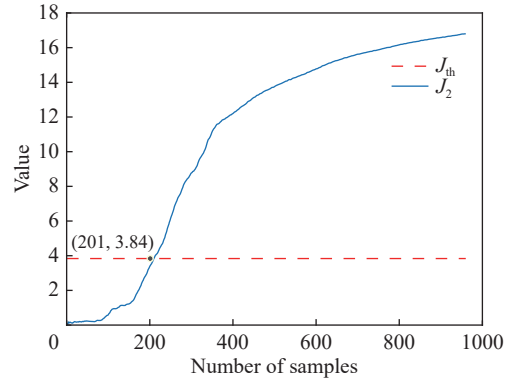

Figure 10 Fault detection result under the optimal threshold.

Table 5 Fault detection result for different thresholds at dc = 200. Bold indicates the best detection result.

Threshold	FDR	FAR
Experience	1.00	0.22
Optimal	**1.00**	**0.00**

V. Conclusion

This paper presents an intelligent fault detection technology based on a data-model interactive compensation mechanism using SIT combined with the MW strategy. The proposed approach effectively addresses the challenges posed by sensor faults in complex industrial environments. Through comprehensive offline and online phases, the method utilizes

data-model interactive compensation to enhance the accuracy and robustness of fault detection. In the offline learning stage, a fault isolation algorithm is used to construct a specific residual for each sensor to isolate the interaction between sensors, and a dynamic optimal threshold is used to maintain an efficient FDR while reducing the FAR, thereby ensuring reliable fault detection. The experiments conducted on the TE process and PT700 bearing load life testing apparatus demonstrate the superior performance of the method. Compared to conventional SIT and MW-SIT approaches, the proposed method shows a significant improvement in sensitivity to sensor faults and robustness against interference. In the future, this method could be combined with other intelligent algorithms and applied to different types of industrial systems to further enhance the intelligence level of fault detection.

ACKNOWLEDGMENT

This work was supported by the National Natural Science Foundation of China (Nos. 62273058 and U22A2045), the Youth Science and Technology Innovation and Entrepreneurship Outstanding Talents Project of Jilin Province (No. 20230508043RC), and the Industrial Technology and Development Special Project of Jilin Provincial Development and Reform Commission (No. 2024C008-2).

REFERENCES

[1] Z. Li, Y. Zhang, J. Ai, Y. Zhao, Y. Yu, and Y. Dong, A lightweight and explainable data-driven scheme for fault detection of aerospace sensors, *IEEE Trans. Aerosp. Electron. Syst*., 2023, 59(6), 8392–8410.

[2] X. Wang and C. P. Tan, Output feedback active fault tolerant control for a 3-DOF laboratory helicopter with sensor fault, *IEEE Trans. Autom. Sci. Eng*., 2024, 21(3), 2689–2700.

[3] H. Chen, H. Luo, B. Huang, B. Jiang, and O. Kaynak, Transfer learning-motivated intelligent fault diagnosis designs: A survey, insights, and perspectives, *IEEE Trans. Neural Networks Learn. Syst*., 2024, 35(3), 2969–2983.

[4] H. Jin, Z. Gao, Z. Zuo, Z. Zhang, Y. Wang, and A. Zhang, A combined model-based and data driven fault diagnosis scheme for lithium-ion batteries, *IEEE Trans. Ind. Electron*., 2024, 71(6), 6274–6284.

[5] X. Yan, M. Sarkar, B. Lartey, B. Gebru, A. Homaifar, A. Karimoddini, and E. Tunstel, An online learning framework for sensor fault diagnosis analysis in autonomous cars, *IEEE Trans. Intell. Transp. Syst*., 2023, 24(12), 14467–14479.

[6] C. Cheng, Y. Ju, S. Xu, Y. Lv, and H. Chen, Local linear generalized autoencoder-based incipient fault detection for electrical drive systems of high-speed trains, *IEEE Trans. Intell. Transp. Syst*., 2023, 24(11), 12422–12430.

[7] G. Li, L. Chen, J. Liu, and X. Fang, Comparative study on deep transfer learning strategies for cross-system and cross-operation-condition building energy systems fault diagnosis, *Energy*, 2023, 263, 125943.

[8] M. Z. Ali, M. N. S. K. Shabbir, X. Liang, Y. Zhang, and T. Hu, Machine learning-based fault diagnosis for single- and multi-faults in induction motors using measured stator currents and vibration signals, *IEEE Trans. Ind. Appl*., 2019, 55(3), 2378–2391.

[9] G. Bode, S. Thul, M. Baranski, and D. Müller, Real-world application of machine-learning-based fault detection trained with experimental data, *Energy*, 2020, 198, 117323.

[10] A. Samanta, S. Chowdhuri, and S. S. Williamson, Machine learning-based data-driven fault detection/diagnosis of lithium-ion battery: A critical review, *Electronics*, 2021, 10(11), 1309.

[11] Q. Zhou, P. Yan, H. Liu, and Y. Xin, A hybrid fault diagnosis method for mechanical components based on ontology and signal analysis, *J. Intell. Manuf*., 2019, 30(4), 1693–1715.

[12] K. Attouri, M. Mansouri, M. Hajji, A. Kouadri, K. Bouzrara, and H. Nounou, Wind power converter fault diagnosis using reduced kernel PCA-based BiLSTM, *Sustainability*, 2023, 15(4), 3191.

[13] S. Wang, Y. Ju, C. Fu, P. Xie, and C. Cheng, A reversible residual network-aided canonical correlation analysis to fault detection and diagnosis in electrical drive systems, *IEEE Trans. Instrum. Meas*., 2024, 73, 3511010.

[14] F. Harrou, K. R. Kini, M. Madakyaru, and Y. Sun, Uncovering sensor faults in wind turbines: An improved multivariate statistical approach for condition monitoring using SCADA data, *Sustain. Energy Grids Networks*, 2023, 35, 101126.

[15] S. X. Ding, P. Zhang, B. Huang, and E. L. Ding, Subspace method aided data-driven design of observer based fault detection systems, *IFAC Proc. Vol*., 2005, 38(1), 167–172.

[16] X. Ding, L. Guo, and T. Jeinsch, A characterization of parity space and its application to robust fault detection, *IEEE Trans. Autom. Control*, 1999, 44(2), 337–343.

[17] Y. Wang, G. Ma, S. X. Ding, and C. Li, Subspace aided data-driven design of robust fault detection and isolation systems, *Automatica*, 2011, 47(11), 2474–2480.

Shenquan Wang received the PhD degree in control science and engineering from Northeastern University, Shenyang, China, in 2014. From 2014 to 2017, he was a postdoctoral research associate at State Key Laboratory of Management and Control for Complex Systems, Institute of Automation, Chinese Academy of Sciences, Beijing, China. From 2021 to 2022, he was an academic visitor at Department of Automation, Tsinghua University, Beijing, China. He is currently a professor at College of Electrical and Electronic Engineering, Changchun University of Technology, Changchun, China. His research interests include robust stability theory, adaptive/distributed control, and complex system security and reliability.

Di Meng received the BS degree in electrical engineering and automation from Changchun University of Technology, Changchun, China, in 2018. He is currently pursuing the MS degree at Changchun University of Technology, Changchun, China. His research interests include fault diagnosis and detection.